Core–shelled Zn/ZnO microspheres synthesised by ultrasonic irradiation for photocatalytic applications

Qing-lan Ma[1], Rui Xiong[1], Bao-gai Zhai[2], Yuan Ming Huang[2]

[1]*School of Physics and Technology, Wuhan University, Hubei 430072, People's Republic of China*
[2]*School of Mathematics and Physics, Changzhou University, Jiangsu 213164, People's Republic of China*
E-mail: dongshanisland@126.com; xiongrui@whu.edu.cn

Published in Micro & Nano Letters; Received on 21st June 2013; Accepted on 9th July 2013

Core–shelled Zn/ZnO microspheres were prepared by ultrasonic irradiation to investigate their photocatalytic activity for degrading methyl orange in waste water. The microstructural and optical properties of the core–shelled Zn/ZnO microspheres were investigated by means of a scanning electron microscope, a transmission electron microscope, an X-ray diffractometer and a photoluminescence spectrometer. The results indicated that the metallic Zn core was about 6 μm in diameter whereas the ZnO shell was about 200 nm in thickness. Owing to the metal–semiconductor junction formed at the Zn/ZnO interface, the core-shelled Zn/ZnO microspheres exhibited higher photocatalytic activity for degrading methyl orange in water when compared with that of ZnO nanoparticles. It suggests that the core–shelled Zn/ZnO microspheres are a promising photocatalyst for the degradation of organic pollutants in water.

1. Introduction: Recently, Zn/ZnO core–shelled microstructures have aroused great interest because of the unique properties of metal–semiconductor junctions formed at the core–shell interface [1–8]. Not only nanometre-scale Zn/ZnO core–shells (i.e. nanodiscs [1], nanodisc dendrites [2], nanotubes [1], nanorods [3] and nanoparticles [4]) but also micrometre-scale Zn/ZnO core–shells (i.e. microspheres [5], microtips [6], microurchins [7] and microcactuses [8]) were prepared by various physical and chemical techniques such as the thermal evaporation method [1, 7, 8], electrodeposition [2, 6], hydrothermal synthesis [3] and laser ablation in liquid medium [4]. These core–shelled structures can have many important features. For example, the metal–semiconductor junction formed at the Zn/ZnO interface can attract electrons from the conduction band of ZnO to the Fermi energy level of the metallic Zn core. Hence, the metallic Zn core acts as an electron-collecting sink while the ZnO nanostructures in the shell provide a large surface area to achieve enhanced photocatalytic activity. Zn/ZnO core–shells with enhanced photocatalytic activity can find wide applications in degrading organic pollutants in waste water. Although the photoluminescence (PL) of the Zn/ZnO core–shells was intensively investigated [1–8], little attention was paid to their photocatalytic properties.

Ultrasound waves can supply the high energy needed for chemical reactions via the process of acoustic cavitations, in which the formation, growth and implosive collapse of bubbles in the liquid are involved. During the implosive collapse of the microcavity, intense local heating of the bubbles occurs within a few microseconds with the result of high-velocity interparticle collisions. The effect generated by the high-velocity interparticle collisions can oxidise the surface layer of the Zn microspheres into ZnO nanostructures. Therefore ultrasonic irradiation is a simple and fast method for large-scale production of Zn/ZnO core–shells at low cost. In this Letter, we report the synthesis and characterisation of Zn/ZnO core–shelled microspheres. The photocatalytic tests show that the Zn/ZnO microspheres have higher photocatalytic activity than ZnO nanoparticles.

2. Experimental details: ZnO nanostructures were synthesised via ultrasonic irradiation in an ultrasonic cleaner. Fine Zn particles with sizes of about 10 μm were purchased from a local chemical supplier. The purity of the Zn powder was higher than 99%. Two grams of metallic Zn particles were added into 200 ml of deionised water in a beaker before the beaker was transferred into an ultrasonic cleaner for the sonochemical reaction. The ultrasonic cleaner consisted of a lead zirconate titanate ultrasonic transducer, a function generator, a power amplifier and a digital multimeter. The disc-shaped transducer was driven at its resonance frequency of 35 kHz with a maximum power output of 100 W. After reaction for 8 h, the grey precipitates at the bottom of the beaker were collected by filtration and rinsed with distilled water and ethanol.

The morphologies, microstructures and PL of the synthesised Zn/ZnO core–shells were characterised with a scanning electron microscope (SEM), X-ray diffraction (XRD), a electron transmission microscope (TEM) and PL spectroscopy, respectively. The details on the instruments and their working parameters were described in our previous reports [9–11]. The evaluation of photocatalytic activity of the core–shelled Zn/ZnO microspheres was performed in a photochemical reactor by degrading methyl orange in water under the illumination of a one 300 W high-pressure mercury lamp. Core–shelled Zn/ZnO microspheres (0.5 g) were dispersed in 100 ml of aqueous solution of methyl orange. The concentration of the aqueous solution of methyl orange was about 10^{-5} M. The aqueous solution of methyl orange was magnetically stirred in the dark for 30 min to ensure the establishment of an adsorption–desorption equilibrium. After having been exposed to ultraviolet (UV) irradiation for a certain period of time, 3 ml of the suspension was collected and then centrifuged to remove the photocatalyst particles. The concentration of methyl orange was determined by checking the absorbance using an UV–visible spectrophotometer.

3. Results and discussion: Ultrasonication generates alternating low-pressure and high-pressure waves in liquids, which in turn lead to the formation and violent collapse of small vacuum bubbles in liquid. Owing to the acoustic cavitation effect, the ultrasonic process is enough to decompose water into H• and •OH radicals [12–14]. This process can be described by the following equation:

$$H_2O \rightarrow H\bullet + \bullet OH \quad (1)$$

Chemical reactions benefit from the free radicals, the energy input and direct mechanical action created by ultrasonic irradiation. When the micrometre-sized Zn particles are present in the water, the effect

of the high-velocity interparticle collisions oxidises the surface layer of the metallic Zn core into ZnO nanostructures. It is predicted that the reactions as described in (2) and (3) take place under ultrasonic treatment

$$Zn + 2e \rightarrow Zn^{2+} \quad (2)$$

$$Zn^{2+} + 2\bullet OH \rightarrow Zn(OH)_2 \rightarrow ZnO + H_2O \quad (3)$$

As a result of these reactions, core–shelled Zn/ZnO microspheres can be produced. Fig. 1 represents the SEM micrographs of the core–shelled Zn/ZnO microspheres (Fig. 1*a* and *b*) and the high-resolution TEM image of the ZnO nanostructures in the shell (Fig. 1*c*). As shown in Fig. 1*a*, the surface of each microsphere is covered with a thin layer of spongy ZnO nanostructures. The typical size of the core–shelled Zn/ZnO microspheres is about 6 μm in diameter. However, the high-velocity interparticle collisions prevent the ZnO shell from growing thick enough because the intense effects generated by the high-velocity interparticle collisions can break the spongy ZnO nanostructures into pieces. That is why only a thin layer of ZnO nanostructures survives on the metallic core. The arrows in Fig. 1*a* locate the fragments of shattered ZnO shells on the surfaces of the Zn/ZnO microspheres. These fragments indicate that the upper limit of the thickness of the shell is about 200 nm. Fig. 1*b* depicts the SEM micrograph of one Zn/ZnO core–shelled microsphere to illustrate the morphology of the ZnO shell. The high-speed impinging liquid jets and the strong hydrodynamic shear-forces in the liquid have removed all fragments of the shattered shell out of the surface of the Zn/ZnO core–shells. The enlarged SEM image shows clearly that nanopores are present in the ZnO shell. To check the nanostructures in the shell, we characterised a piece of the shattered shell with high resolution TEM. Fig. 1*c* depicts the high-resolution TEM image of the ZnO nanostructures in the shell. It is obvious that the shell is composed of many ZnO nanoparticles, whose sizes are in the range of 2–5 nm. The measured spacing between two adjacent planes of the ZnO nanoparticles is about 0.26 nm, which is consistent with the standard spacing between two adjacent 002 planes of hexagonal ZnO.

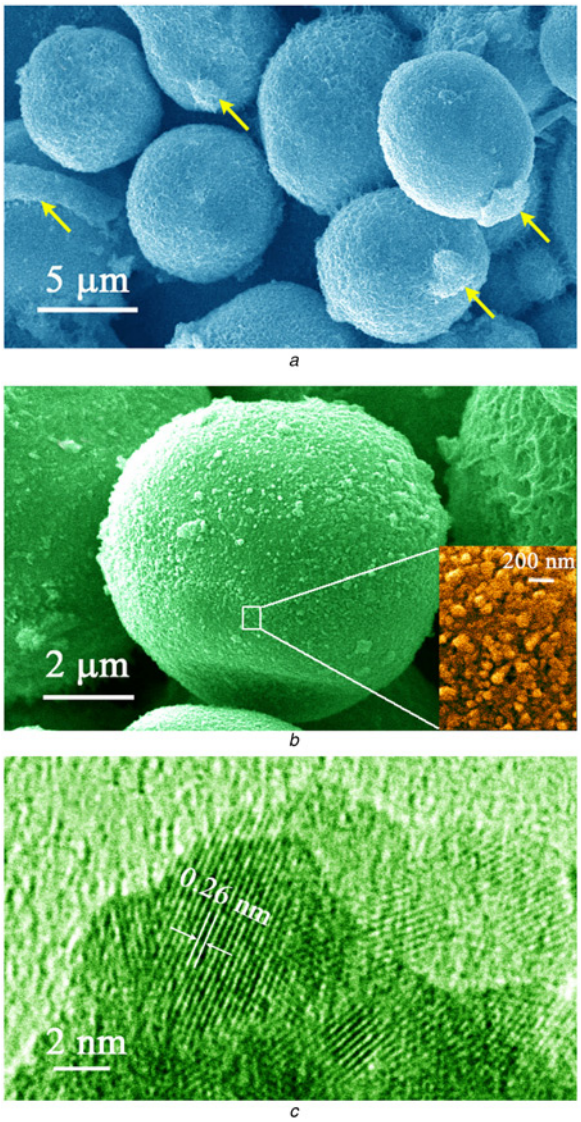

Figure 1 *SEM micrographs of core–shelled Zn/ZnO microspheres and high-resolution TEM image of ZnO nanostructures in shell*
a, *b* SEM micrographs
c High-resolution TEM image

Fig. 2 gives the powder XRD curves of the core–shelled Zn/ZnO microspheres. The peaks at 31.74°, 34.36°, 36.22°, 47.54°, 56.58°, 62.86°, 66.32°, 67.90° and 69.02° in Fig. 2 can be assigned to the reflections from the 100, 002, 101, 102, 110, 103, 200, 112 and 201 planes of the hexagonal ZnO (JCPDS No. 36–1451). The peaks at 36.296°, 38.992°, 43.231°, 54.336°, 70.056°, 70.660° and 77.027° can be assigned to the reflections from 002, 100, 101, 102, 103, 110 and 004 planes of the hexagonal Zn (JCPDS No. 04–0831). It is clear that both the peaks of Zn and ZnO are present in Fig. 2. Therefore the data in Fig. 2 confirm that the Zn/ZnO composite was synthesised via ultrasonic irradiation.

Fig. 3 illustrates the room temperature PL spectra of the core–shelled Zn/ZnO microspheres prepared by ultrasonic irradiation for 6, 8 and 10 h. As shown in Fig. 3, each PL curve is composed of a UV PL band and a green PL band. As the ultrasonic reaction time was varied in the range of 6–10 h, the peak positions of the

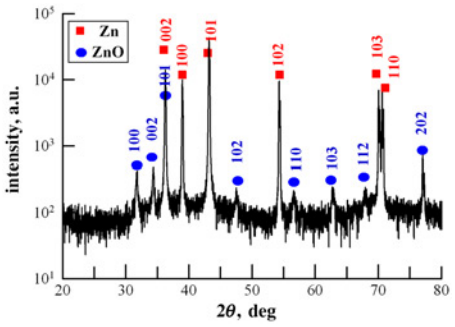

Figure 2 *Powder XRD curve of core–shelled Zn/ZnO microspheres*

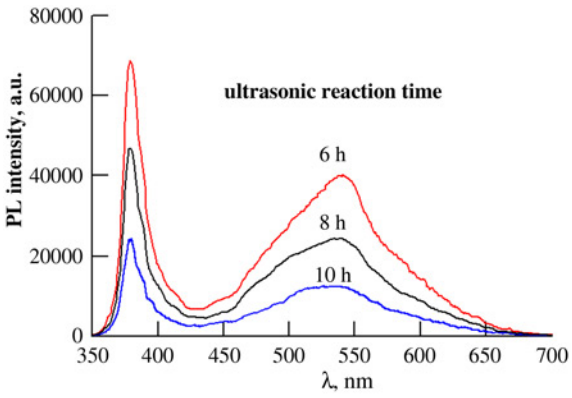

Figure 3 *Room temperature PL spectra of core–shelled Zn/ZnO microspheres prepared by ultrasonic irradiation for 6, 8, 10 h*

doi: 10.1049/mnl.2013.0394

UV PL band and the green PL band were pinned at 380 and 540 nm, respectively. It is well established that the UV PL band of the ZnO nanostructures originates from free excitonic recombination whereas the green PL band can be attributed to the singly ionised oxygen vacancies [9–11]. The relative intensities of the green PL band to that of the UV PL band did not change too much; the calculated chromatic coordinates in the CIE 1931 *XYZ* space were about (0.27, 0.45) for each of the three PL curves [15, 16]. These data suggest that the intrinsic defect densities in the ZnO shell are not sensitive to the ultrasonic reaction time. The consistency of the recorded PL spectra in Fig. 3 with those reported in the literature gives additional evidence on the formation of ZnO nanostructures in the shell [17]. More importantly, the emission efficiency of the ZnO nanostructures in the shell is lowered by the formation of a metal–semiconductor junction at the Zn–ZnO interface because a portion of electrons in ZnO can be attracted to the metallic Zn core [18].

The photocatalytic activity of the Zn/ZnO core–shell microspheres was evaluated by the degradation of methyl orange under UV light irradiation. Fig. 4 illustrates the absorption spectra of the aqueous solution of methyl orange in the presence of the core–shelled Zn/ZnO microspheres. Before UV irradiation, methyl orange exhibits a strong absorption at about 464 nm and a weak absorption at about 268 nm. The strong absorption at 464 nm is generally attributed to the big π system formed by the two separated phenyls and the azo linkage in the methyl orange molecule. The absorption at about 268 nm can be assigned to the phenyl chromophores in the dye molecule [19]. After UV irradiation for 10 min, the absorption at 464 nm decreases in intensity whereas the absorption at 265 nm disappears. The decrease in the absorption at 464 nm indicates that the azo linkages in some dye molecules are cleaved [20, 21], the disappearance of the absorption at 265 nm suggests that the phenyl chromophores in the dye are broken or oxidised by the photocatalyst. Furthermore, we note that a new absorption appears at about 242 nm after UV irradiation for 10 min. Comparison with the absorption data in the Hazardous Substance Data Bank shows that this new absorption cannot be attributed to the fragments of the dye molecules including benzene, *N*,*N*-dimethylaniline, *N*,*N*-dimethyl-*p*-nitrosoaniline, *N*,*N*-dimethyl-*p*-benzenediamine or sodium benzosulfonate. Instead, the new absorption at 242 nm probably originates from the small molecule phenylcarbamic acid (phenyl–NH–COOH) whose absorption peaks at about 240 nm [21]. Hence, the appearance of the absorption at about 242 nm reveals that one kind of small molecule is generated in the process of photodegradation. As the UV irradiation is prolonged, the absorption at 464 nm is gradually decreased to a very low level, whereas the absorption at 242 nm is increased to a high level. Such changes in the absorptions suggest that more and more dye molecules are broken into small fragments.

According to the definition given by the International Union of Pure and Applied Chemistry in 1996, photodegradation is the photochemical transformation of a molecule into lower molecular weight fragments, usually in an oxidation process. That is why the change in the absorption at about 464 nm has been widely employed to quantitatively characterise the photodegradation of methyl orange [20, 21]. Therefore the results in Fig. 4 indicate that the core–shelled Zn/ZnO microspheres are an active photocatalyst. As shown in Fig. 4, about 94% methyl orange in water was degraded by the core–shelled Zn/ZnO microspheres under UV irradiation for 120 min. For comparison, direct photolysis of methyl orange degradation in the absence of the Zn/ZnO core–shells was performed under identical conditions. As shown by the inset of Fig. 4, methyl orange concentration in the absence of Zn/ZnO core–shelled microspheres was hardly changed with the increase of UV irradiation time. To compare the photocatalytic activity of the core–shelled Zn/ZnO microspheres with that of ZnO nanoparticles, we calculated the weight of the ZnO nanostructures in 0.5 g of core–shelled microspheres by taking the typical values of the radius of Zn core (3 μm) and the thickness of the ZnO shell (200 nm). Our calculated ZnO weight was about 0.067 g. Under identical conditions, only 60% methyl orange in water was degraded by 0.067 g of ZnO nanoparticles under UV irradiation for 120 min. It demonstrates that the photocatalytic activity of the core–shelled Zn/ZnO microspheres has been enhanced.

The enhanced photocatalytic activity can be attributed to the metal–semiconductor junction formed at the Zn–ZnO interface. Since the photocatalytic process of Zn/ZnO core–shells is complex, it is necessary to discuss the band structure of core–shelled Zn/ZnO microspheres in detail. Fig. 5 represents the band structure of the Zn/ZnO core – shelled microspheres. The work function of Zn (4.3 eV) was taken from Lide [22], whereas the electron affinity of ZnO (4.5 eV) was taken from Jacobi *et al.* [23] and Gupta *et al.* [24]. When the catalysts are irradiated by UV light with photon energy higher than or equal to the bandgap of ZnO nanocrystals, electrons in the valence band will be excited to the conduction band with simultaneous generation of the same amount of holes in the valence band. As presented in Fig. 5, the bottom energy level of the conduction band of ZnO is higher than the Fermi energy level of the metallic Zn core, therefore the photoexcited electrons can transfer from the conduction band of ZnO to the Fermi level of the Zn core under the driving force of the potential energy [18]. Subsequently, electronic acceptors, such as adsorbed O_2, can easily trap photoelectrons to produce a superoxide anion radical ($\bullet O_2^-$), whereas the photoinduced holes can readily react with surface bound OH^- to generate hydroxyl radical species ($\bullet OH$). The latter is an extremely strong oxidant for degeneration of organic chemicals.

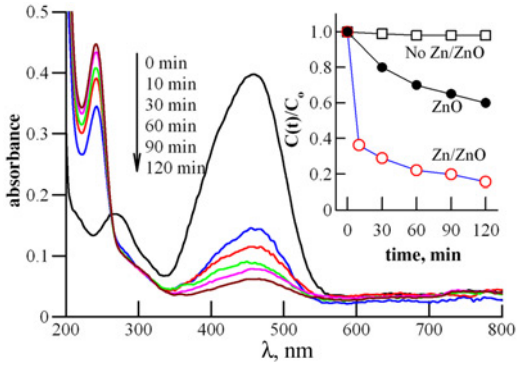

Figure 4 *Absorption spectra of aqueous solution of methyl orange in presence of core–shelled Zn/ZnO microspheres under UV irradiation for different times*

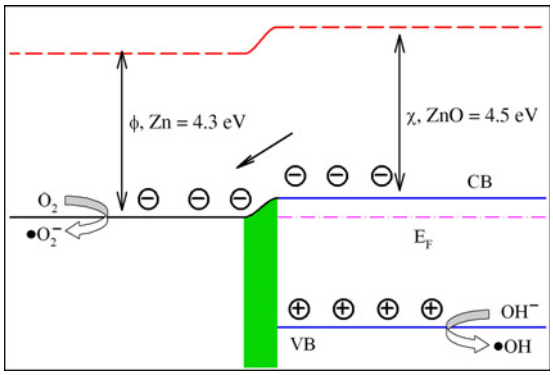

Figure 5 *Band structure of core–shelled Zn/ZnO microspheres to show photocatalytic reactions*

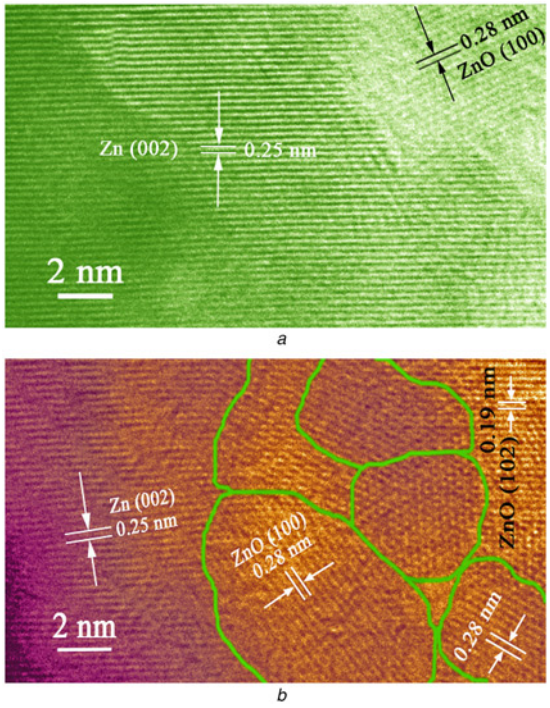

Figure 6 *High-resolution TEM images to show interfaces between Zn core and ZnO shell*

As discussed above, the Zn–ZnO interface plays an important role in the photocatalytic activity of the Zn/ZnO microspheres. Fig. 6 shows the high-resolution TEM images of the Zn–ZnO interface. The interface between one ZnO nanoparticle and the Zn core is illustrated in Fig. 6*a*. The Zn core takes the (002) crystal orientation. As a contrast, the ZnO nanoparticle takes the (100) crystal orientation. The angle between the two sets of crystal orientations is about 30°, and the lattice distortion at the Zn–ZnO interface can be seen clearly in Fig. 6*a*. The interfaces between the Zn core and multiple ZnO nanoparticles are shown in Fig. 6*b*. The interfaces between the multiple ZnO grains are marked with heavy lines. The Zn core takes the (002) crystal orientation whereas the ZnO nanoparticles take various crystal orientations such as (100) and (102). The crystal orientations of the ZnO nanoparticles are tilted to that of the Zn core. The effect of the high-velocity interparticle collisions and strong hydrodynamic shear-forces in the liquid are responsible for the tilted crystal lattices of the grown ZnO nanoparticles.

The dense ZnO nanoparticles in the shell can generate a significant effect on the photocatalytic activity of the core–shelled Zn/ZnO microspheres. If the Zn core stands alone in environments such as the photocatalysis, the surface of the metal Zn particles will be oxidised into ZnO. This situation is changed when the Zn core is covered with a thin layer of ZnO nanostructures because the dense ZnO nanostructures in the shell can passivate the surface of the metallic Zn core and protect the core against further oxidation and corrosion in some environments. Our tests showed that the loss in photodegradation efficiency of the catalyst was less than 10% after the catalysts had been repeatedly used for 15 catalytic cycles. The limited loss in the photodegradation efficiency demonstrates that the synthesised catalyst is reasonably stable for multiple photocatalytic cycles.

4. Conclusions: Metal–semiconductor Zn/ZnO core–shelled microspheres have been synthesised by ultrasonic irradiation in an ultrasonic cleaner. The synthesised materials have been characterised by means of SEM, TEM, XRD, PL and UV–visible absorption spectroscopy. One Zn/ZnO core–shell is composed of a metallic Zn core (6 μm in diameter) and one 200 nm-thick ZnO shell. Our results have demonstrated that the core–shelled Zn/ZnO microspheres can exhibit higher photocatalytic activity than ZnO nanoparticles. Electron migration from the ZnO shell to the metallic Zn core is responsible for enhanced photocatalytic activity. The enhanced photocatalytic activity would allow the Zn/ZnO core–shelled microspheres to gain wide applications in degrading organic pollutants in water. Owing to its simplicity, short reaction time and low-energy consumption, the ultrasonication method can be utilised for mass production of various kinds of Zn/ZnO core–shells at low cost.

5 References

[1] Gao P.X., Lao C.S., Ding Y., Wang Z.L.: 'Metal/semiconductor core/shell nanodisks and nanotubes', *Adv. Funct. Mater.*, 2006, **16**, pp. 53–62

[2] Zhang X.Y., Dai J.Y., Lam C.H., *ET AL.*: 'Zinc/ZnO core–shell hexagonal nanodisk dendrites and their photoluminescence', *Acta Mater.*, 2007, **55**, pp. 5039–5044

[3] Trejo M., Santiago P., Sobral H., Rendón L., Pal U.: 'Synthesis and growth mechanism of one-dimensional Zn/ZnO core–shell nanostructures in low-temperature hydrothermal process', *Cryst. Growth Des.*, 2009, **9**, pp. 3024–3030

[4] Zeng H., Li Z., Cai W., Cao B., Liu P., Yang S.: 'Microstructure control of Zn/ZnO core/shell nanoparticles and their temperature-dependent blue emissions', *J. Phys. Chem. B*, 2007, **111**, pp. 14311–14317

[5] Lupan O., Chow L., Chai G., Heinrich H.: 'Fabrication and characterization of Zn/ZnO core–shell microspheres from nanorods', *Chem. Phys. Lett.*, 2008, **465**, pp. 249–253

[6] Kuan C.Y., Chou J.M., Leu I.C., Hon M.H.: 'Self-organized Zn/ZnO core–shelled hierarchical structures prepared by aqueous chemical growth', *J. Mater. Res.*, 2008, **23**, pp. 1163–1167

[7] Tang D.M., Liu G., Li F., *ET AL.*: 'Synthesis and photoelectrochemical property of urchin-like Zn/ZnO core–shell structures', *J. Phys. Chem. C*, 2009, **113**, pp. 11035–11040

[8] Khan W.S., Cao C., Chen Z., Nabi G.: 'Synthesis, growth mechanism, photoluminescence and field emission properties of metal–semiconductor Zn/ZnO core–shell microcactuses', *Mater. Chem. Phys.*, 2010, **124**, pp. 493–498

[9] Ma Q.L., Zhai B.G., Huang Y.M.: 'Sol–gel derived ZnO/porous silicon composites for tunable photoluminescence', *J. Sol-Gel Sci. Technol.*, 2012, **64**, pp. 110–116

[10] Huang Y.M., Ma Q.L., Zhai B.G.: 'Wavelength tunable photoluminescence of ZnO/porous Si nanocomposites', *J. Lumin.*, 2013, **138**, pp. 157–163

[11] Huang Y.M., Ma Q.L., Zhai B.G.: 'A simple method to grow one-dimensional ZnO nanostructures in air', *Mater. Lett.*, 2013, **93**, pp. 266–268

[12] Li H., Liu E.T., Chan F.Y.F., Lu Z., Chen R.: 'Fabrication of ordered flower-like ZnO nanostructures by a microwave and ultrasonic combined technique and their enhanced photocatalytic activity', *Mater. Lett.*, 2011, **65**, pp. 3440–3443

[13] Oh E., Jung S.H., Lee K.H., Jeong S.H., Yu S.G., Rhee S.J.: 'Vertically aligned Fe-doped ZnO nanorod arrays by ultrasonic irradiation and their photoluminescence properties', *Mater. Lett.*, 2008, **62**, pp. 3456–3458

[14] Pholnak C., Sirisathitkul C., Harding D.J.: 'Characterizations of octahedral zinc oxide synthesized by sonochemical method', *J. Phys. Chem. Solids*, 2011, **72**, pp. 817–823

[15] Ma Q.L., Xiong R., Huang Y.M.: 'Tunable photoluminescence of porous silicon by liquid crystal infiltration', *J. Lumin.*, 2011, **131**, pp. 2053–2057

[16] Zhai B.G., Huang Y.M.: 'Quantitative determination of color coordinates for lumninescent materials', *Solid State Phenom.*, 2012, **181–182**, pp. 285–288

[17] Ma Q.L., Xiong R., Huang Y.M.: 'Ultrasonication induced synthesis of Zn/ZnO core–shell structures', *Key Eng. Mater.*, 2013, **538**, pp. 185–188

[18] Liu H.R., Shao G.X., Zhao J.F., *ET AL.*: 'Worm-like Ag/ZnO core–shell heterostructural composites: fabrication, characterization and photocatalysis', *J. Phys. Chem. C*, 2012, **116**, pp. 16182–16190

doi: 10.1049/mnl.2013.0394

[19] Berllman I.B.: 'Handbook of fluorescence spectra of aromatic molecules' (Academic Press, New York, 1971, 2nd edn), p. 111
[20] Kaur J., Bansal S., Singhal S.: 'Photocatalytic degradation of methyl orange using ZnO nanopowders synthesized via thermal decomposition of oxalate precursor method', *Phys. B*, 2013, **416**, pp. 33–38
[21] Hong R.Y., Li J.H., Chen L.L., *ET AL.*: 'Synthesis, surface modification and photocatalytic property of ZnO nanoparticles', *Powder Technol.*, 2009, **189**, pp. 426–432
[22] Lide D.R.: 'Handbook of chemistry and physics' (CRC Press, Boca Raton, 2000, 82nd edn), pp. 12–124
[23] Jacobi K., Zwicker G., Gutmann A.: 'Work function, electron affinity and band bending of zinc oxide surfaces', *Surf. Sci.*, 1984, **141**, pp. 109–125
[24] Gupta B., Jain A., Mehra R.M.: 'Development and characterization of sol–gel derived Al doped ZnO/p-Si photodiode', *J. Mater. Sci. Technol.*, 2010, **26**, pp. 223–227